Mon. Not. R. Astron. Soc. **271,** 31–38 (1994)

A search for weak distortion of distant galaxy images by large-scale structure

Jeremy Mould,[1] Roger Blandford,[2] Jens Villumsen,[3] Tereasa Brainerd,[2] Ian Smail,[1] Todd Small[1] and William Kells[4]

[1] *Palomar Observatory, Caltech 105-24, Pasadena, CA 91125, USA*
[2] *Theoretical Astrophysics, Caltech 130-33, Pasadena, CA 91125, USA*
[3] *The Ohio State University, Department of Astronomy, 174 W. 18th Avenue, Columbus, OH 43210, USA*
[4] *The Observatories of the Carnegie Institute of Washington, 813 Santa Barbara Street, Pasadena, CA 91101, USA*

Accepted 1994 May 24. Received 1994 May 12; in original form 1993 November 22

ABSTRACT

We have completed a feasibility study for the measurement of weak distortion of distant galaxy images by intervening large-scale structure by using the 5-m Hale reflector to acquire a very deep, $r \sim 26$, exposure of a single field. The error budget of our observations is dominated by the effects of atmospheric seeing (which strongly degrades this signal because the faintest images are under-resolved) and telescope effects. After performing a correction for telescope aberrations and possible guiding errors, the observed mean 'polarization' of the images of 4363 galaxies with magnitudes $23 \leq r \leq 26$ within a circle of radius 4.8 arcmin was found to be $\overline{p} = 0.01 \pm 0.01$. The associated two-point polarization correlation function has a constant value of $C_{pp} = (1.4 \pm 3.0) \times 10^{-5}$ over the angular range 1 to 6 arcmin. It is predicted that the cosmological polarization should be in the range $p = 0.03 \pm 0.01$ for a standard CDM universe normalized by a bias parameter, b, of unity (p scales inversely with b and approximately linearly with Ω_0). For the atmospheric seeing and sky noise conditions associated with our data, Monte Carlo simulations suggest that the efficiency of measuring the mean cosmological polarization is on the order of 40 ± 10 per cent. Thus our preliminary analysis suggests an upper limit on the cosmological mean polarization in the field of $\overline{p}_{max} \sim 0.04$. Deep wide-field imaging in 0.5 arcsec seeing to study this polarization signal should provide limits that constrain current cosmological models.

Key words: polarization – galaxies: photometry – cosmology: observations – gravitational lensing – large-scale structure of Universe.

1 INTRODUCTION

The prediction that cosmologically distant, discrete galaxies and rich clusters could act as gravitational lenses (e.g. Zwicky 1937) became observational reality with the discovery that Q0957+561 was multiply imaged (Walsh, Carswell & Weymann 1979). To date, over 30 examples of this phenomenon, including radio rings and giant arcs, have been discovered (e.g. Schneider, Ehlers & Falco 1992; Blandford & Narayan 1992). Equally intriguing is the notion that weak lensing, equivalent to a systematic, induced image ellipticity without multiple imaging, might be used as a probe of large-scale inhomogeneity in the distribution of matter (e.g. Kristian 1967; Gunn 1967). In essence, when rays from a distant galaxy pass by an overdensity in the matter distribution, the observed images will be marginally elongated tangentially with respect to the centre of the perturbation, as has been clearly observed with several rich clusters (e.g. Tyson, Valdes & Wenk 1990; Fort et al. 1991; Smail et al. 1994). Underdensities will produce a radial elongation. Independent perturbations along the line of sight will add stochastically (Blandford et al. 1991; Miralda-Escudé 1991; Kaiser 1992). Early searches for this effect outside rich clusters (Kristian 1967; Valdes, Tyson & Jarvis 1983) led to unsurprising non-detections. However, two recent observational developments motivate a new attempt, and this paper is a report on one such effort.

The first observational development is that there appears to be more inhomogeneity in the cosmological distribution of luminosity than had been expected. For example, Huchra et

al. (1988) found that galaxies in the CFA redshift survey were concentrated near the 'walls' of large ~ 100-Mpc voids. (Throughout this paper, we shall assume an Einstein–de Sitter universe with a Hubble constant of $H_0 = 50$ km s^{-1} Mpc^{-1}.) In addition, Saunders et al. (1991) measured a larger power in the two-point correlation function for galaxies on scales ~ 50 Mpc than was anticipated on the basis of a cold dark matter (CDM) cosmogony. The measurement of the cosmic microwave background fluctuations by *COBE* on angular scales $\gtrsim 7°$ (Smoot et al. 1992) also indicates an increase in contemporary density perturbations to about twice the size of what had previously been expected. The *COBE* result increases the anticipated weak gravitational lensing 'signal' to a mean correlated ellipticity ~ 0.03 for sources at $z \sim 1$.

Secondly, there has been a large increase in the expected number of imageable galaxies. Following the work of, for example, Tyson (1988), Lilly, Cowie & Gardner (1991) and Metcalfe et al. (1993), the measured surface density of galaxies is $\gtrsim 2.3 \times 10^5$ per square degree by $r \sim 26$, nearly an order of magnitude in excess of the number expected on the basis of the measured local density of bright galaxies. The recent availability of large format CCDs on 4-m class telescopes makes it practical to undertake well-sampled measurements of the observed ellipticities of $\sim 10^4$ faint galaxies, reducing the 'noise' to an rms intrinsic image ellipticity of ~ 0.003 per field, as well as allowing exploration of the various systematic errors associated with telescope and atmosphere-induced ellipticities. Furthermore, the steady increase in the median redshift of galaxies with magnitude to depths of $B \lesssim 24$ (e.g. Ellis 1993), coupled with results on the observed lensing strength of rich clusters as a function of their redshift (Smail et al. 1994), suggests that the majority of these faint galaxies have $z \sim 1$.

In this paper, we re-calculate the expected weak distortion due to large-scale structure and report on a pilot project conducted on a single 9.6×9.6 arcmin^2 field using the 5-m Hale reflector. Although our current results are inconclusive, we argue that it ought to be possible to perform this measurement with confidence under conditions of superior seeing with a well-controlled telescope.

In Section 2 of this paper, we present a brief, updated theoretical summary of the effect that we seek. Section 3 describes the observations and their reduction. In Section 4, we discuss the model predictions and describe Monte Carlo simulations designed to quantify the influence of telescope and atmosphere-induced aberrations and noise sources. In Section 5, we analyse our results and compare them with the model predictions through the Monte Carlo simulations.

2 THEORETICAL PREDICTION OF 'POLARIZATION'

We introduce angular coordinates θ_1, θ_2 along the directions of decreasing right ascension and increasing declination (in the northern hemisphere), respectively. If the gravitational distortion displaces an image point by $\delta\theta$, then the complex 'polarization' $p(\theta)$ is defined in terms of the mean distortion measured over a distribution of sources with redshift z and comoving distance $x = 2c[1-(1+z)^{-1/2}]/H_0$. To linear order, in an Einstein–de Sitter universe, this is predicted to be

$$p(\theta_1, \theta_2) = \delta\theta_{2,2} - \delta\theta_{1,1} - 2\mathrm{i}\delta\theta_{1,2} = 2\int_0^2 \mathrm{d}x \frac{w(x)}{x}(\phi_{,22} - \phi_{,11} - 2\mathrm{i}\phi_{,12}), \quad (1)$$

where $w(x) = \int_x^2 \mathrm{d}x' g(x')(1 - x/x')$ is the source weight function [with $g(x)$ being the normalized galaxy distribution function per unit x and per unit solid angle], ϕ is the local Newtonian potential and a comma denotes differentiation with respect to $\theta_{1,2}$ (Blandford & Jaroszyński 1981; Blandford et al. 1991; Miralda-Escudé 1991; Kaiser 1992). If we let $\tilde{\delta}(\boldsymbol{k})$ be the Fourier transform of the contemporary relative density perturbation and assume linear growth, proportional to $(1+z)^{-1}$, then

$$p(\theta_1, \theta_2) = -3\int_0^2 \mathrm{d}x\, w(x) x \int \frac{\mathrm{d}^3k}{(2\pi)^3} \mathrm{e}^{\mathrm{i}(\boldsymbol{k}\cdot\boldsymbol{x} + 2\psi)} \tilde{\delta}(\boldsymbol{k}), \quad (2)$$

where $\psi = \tan^{-1}(k_2/k_1)$.

The simplest statistic to compute and compare with observation is the mean polarization, $\bar{p}$, within a circular aperture of angular radius θ_0 centred on the CCD frame:

$$\bar{p} = \frac{1}{\pi\theta_0^2}\int_0^{\theta_0} \mathrm{d}\theta\,\theta \int_0^{2\pi} \mathrm{d}\alpha\, p(\theta\cos\alpha, \theta\sin\alpha) = -3\int_0^2 \mathrm{d}x\, w(x) x \int \frac{\mathrm{d}^3k}{(2\pi)^3} \mathrm{e}^{\mathrm{i}(k_3 x + 2\psi)} \left[\frac{2J_1(k\theta_0 x)}{k\theta_0 x}\right] \tilde{\delta}(\boldsymbol{k}). \quad (3)$$

This statistic allows the accumulation of data taken with different orientations and the exclusion of galaxy images near the corners of the frame where telescope aberration may be most extreme. Averaging over an ensemble of apertures, we obtain the mean square polarization

$$\langle|\bar{p}|^2\rangle = 36\pi^2 \int \mathrm{d}k\, k P(k) \int_0^2 \mathrm{d}x\, w(x)^2 x^2 \left[\frac{2J_1(k\theta_0 x)}{k\theta_0 x}\right]^2, \quad (4)$$

where $P(k)$ is the power spectrum of relative density fluctuations.

An associated quantity is the two-point polarization correlation function

$$C_{\mathrm{pp}}(\theta) = \langle p(\theta) p^*(0)\rangle = 36\pi^2 \int \mathrm{d}k\, k P(k) \int_0^2 \mathrm{d}x\, x^2 w(x)^2 J_0(kx\theta) \quad (5)$$

(Blandford et al. 1991). The extension to a general Friedmann–Robertson–Walker universe is reasonably well approximated by simply scaling the polarization with the density parameter Ω_0 (Villumsen et al., in preparation).

By adopting $\theta_0 = 4.8$ arcmin, to match our data set (see Section 3), and the CDM power spectrum of Davis et al. (1985), we have computed $\bar{p}_{\mathrm{rms}} = \langle|\bar{p}|^2\rangle^{1/2}$ for a variety of choices of $g(x)$. (Note that we normalize the CDM power spectrum by a bias parameter, b, of unity, to accommodate the *COBE* microwave background fluctuations.) If, to take an extreme example, all source galaxies are at a redshift $z = 3$, we find $\bar{p}_{\mathrm{rms}} = 0.076$. More realistically, if the source galaxies are distributed out to $z = 3$ (cf. Guhathakurta, Tyson & Majewski 1990) with $g(x) = 30x^2(1-x)^2$, and a median redshift $z_{\mathrm{m}} = 0.8$, then $\bar{p}_{\mathrm{rms}} = 0.030$. This source distribution

is roughly that expected if the no-evolution models which fit at brighter magnitudes are extrapolated to our limit (Lilly 1993, Glazebrook et al., in preparation). For $g(x)=12x^2(1-x)$, $60x^2(1-x)^3$ and $z_m=1.1$, 0.6, respectively, $\overline{p}_{rms}=0.038$, 0.025, indicating a significant sensitivity to the redshift distribution. (The computed predictions for C_{pp}(4.8 arcmin) for these three trial galaxy distribution functions are 2.1×10^{-4}, 2.9×10^{-4} and 1.6×10^{-4}, respectively.)

The choice of this particular circular aperture, $\theta_0=4.8$ arcmin, probes fluctuations over a certain range of length-scales. Assuming the CDM spectrum, between 70 and 80 per cent of the signal is contributed by waves with $0.1<k<1$ Mpc^{-1}. Waves with $k\gtrsim0.2$ Mpc^{-1} are of non-linear amplitude now, however, and therefore did not grow linearly in the recent past. Using the non-linear evolution of the mass power spectrum from an N-body simulation of a standard CDM universe (Brainerd & Villumsen 1994), we find ~10 per cent increase in the mean polarization and ~50 per cent increase in C_{pp}(4.8 arcmin) [$\overline{p}_{rms}=0.042$, 0.030, 0.028 and $C_{pp}=4.0\times10^{-4}$, 3.2×10^{-4}, 2.6×10^{-4} for $g(x)=12x^2(1-x)$, $30x^2(1-x)^2$, $60x^2(1-x)^3$, respectively].

In summary, it is reasonable to expect a mean polarization in the range 0.03 ± 0.01 in the absence of any systematic observational biases.

We note that galaxies have been reported (Binggeli 1982) to be aligned over scales of order 10 Mpc, but the amplitude and correlation length of this alignment are uncertain. Such alignments can mimic a cosmological gravitational lensing effect. However, because galaxies are observed over a path-length of several Gpc, any effect will tend to be averaged out. As a simple illustrative model, assume that the major axes of galaxies are correlated over a length-scale L, in units of h^{-1} Mpc, with a mean polarization $\langle p\rangle$. If $g(x)=30x^2(1-x)^2$, then $\overline{p}=0.015\,|\langle p\rangle|\,L^{1/2}$. For reasonable values of $\langle p\rangle$ and L, $\overline{p}$ is much less than 1 per cent. Another possibility for a spurious signal occurs if the line of sight intercepts a cluster or supercluster where galaxies tend to align with the major axis. Our field was specifically chosen to avoid such clusters and, furthermore, an intervening cluster would generate a related excess in the observed number counts (cf. Blandford et al. 1991), and no such excess is observed in the data.

3 OBSERVATIONS AND REDUCTION

The observations for this project were taken with COSMIC at the prime focus of the 5-m Hale telescope. The COSMIC instrument is an efficient, high-throughput wide-field imaging spectrograph with a thinned, antireflection-coated Tektronix 2048^2 chip as detector (Dressler & Kells 1993). The field of view is 9.6×9.6 arcmin^2 at a scale of 0.28 arcsec pixel^{-1}, allowing critical sampling of all but the best seeing available at Palomar. The main data set consists of a 26.5-ks integration on a single blank field (centred on Hercules-2, $\alpha(1950)=17^h2107^s$, $\delta(1950)=+49°52'21''$) taken in Gunn r. The field was observed as it transited on the nights of 1992 May 29, June 8–10 and August 3. The seeing during these periods ranged from 0.7 to 0.9 arcsec. These data are primarily intended to select targets for a very faint galaxy redshift survey to be undertaken with the Keck telescopes. Additional, shallower g and i exposures are available and provide colour information on the objects detected in the deep r image. The observing conditions (seeing and transparency) across these nights were uniformly good and stable.

The observations consist of multiple, ~1000-s exposures (giving approximately 20 000 e$^-$ per pixel from the sky) with the telescope offset between exposures. This technique allows us to construct colour-matched flat-field frames from suitably processed data frames. To test for possible systematic errors induced by the telescope and CCD, the observations were taken at a number of position angles on the sky to allow their easy identification.

The data were reduced using standard IRAF procedures. The frames were first debiased and trimmed and had a small number of bad columns removed by interpolation. The data frames were then initially flat-fielded with dome-flats. This facilitates the use of an image detection package (FOCAS, Jarvis & Tyson 1981) to detect and then remove all stars and galaxies. The areas occupied by such sources are replaced with values randomly drawn from the surrounding sky. These cleaned frames are then copied, the copies being heavily smoothed. The cleaned frames are divided by the smoothed copies to leave just the pixel-to-pixel response of the chip. For each data frame, a flat-field is constructed by combining the pixel response frames of all the other data frames from that night. The data frame is first flat-fielded with this master flat-field, before having residual large-scale sensitivity gradients removed by dividing through by its smoothed cleaned copy. This method produces frames that are both flat and have minimal pixel-to-pixel noise.

All suitably processed frames were then geometrically remapped to remove residual distortion in the field corrector (see below), rotated and aligned to a single fiducial basis (absolute alignment tolerance 0.01 arcsec). A frame-by-frame comparison of the positions of bright stellar reference objects showed incoherent displacement vectors with an rms scale of 0.03 arcsec. Two frames had distortion patterns well in excess of this figure and these were discarded before combining the remainder with a cosmic-ray rejection filter to produce the final image. This frame covers 90.0 arcmin^2, has a total integration time of 24.0 ks and a 1σ surface-brightness limit of $\mu_r=28.8$ mag arcsec^{-2}. The seeing measured from stars in this frame is 0.87 arcsec.

FOCAS was then used to detect objects using combined isophotal and minimum area thresholds (equivalent to the average surface brightness over the seeing disc exceeding $\mu_r=27.3$ mag arcsec^{-2}). We select only those objects classed as either stars or galaxies by FOCAS's image classifier – these constitute 98.9 per cent of the objects detected. The catalogue contains ~6000 objects brighter than the 95 per cent completeness limit of the frame of $r=26.0$. At this limit, the average photometric errors are $\Delta r\sim0.15$ mag, with the faintest objects corresponding to a 14σ detection within the seeing disc (4.5σ in our minimum 3.0-arcsec photometry aperture). Statistically reliable ellipticities ($\Delta\varepsilon\sim0.10$) are available to our adopted completeness limit from the intensity-weighted second moments calculated by FOCAS. To provide a control sample with which to estimate systematic biases in our polarization measurement, a set of isolated bright stars was also selected from the final catalogue.

The final catalogue of objects contains 4363 objects with $23<r<26$ within a circle of radius 4.8 arcmin centred on our field. A fit to the differential galaxy counts per square degree from this field gives $\log(dN/dr)=(0.307\pm$

$0.007)r - 3.06 \pm 0.16$, in good agreement with the slope proposed by Steidel & Hamilton (1993) from significantly shallower data.

4 ANALYSIS

When comparing the observations with theoretical predictions, it is apparent that a number of effects can either degrade or artificially enhance a cosmological weak lensing signal, resulting in an observed signal that may differ significantly from the intrinsic signal. Processes that would degrade the signal include seeing, sky noise effects on the detected image isophotes, image crowding, and undetected merged galaxy images. An artificial signal could be created by either poor guiding of the telescope or aberrations in the optics. Finally, the object detection and analysis procedure may also introduce biases and these too must be modelled. Some of these effects can be removed from the data set after accurate calibration. Others, however, cannot be easily corrected for in the data and it is therefore necessary to create simulated images to calibrate the likely effect of these processes on the theoretical predictions.

4.1 Telescope aberration

One obvious source of systematic error is aberration of the images due to the primary mirror and the COSMIC imager. In order to quantify these effects, we analysed several offset images of the outskirts of the globular cluster M3. A globular cluster field provides us with a large sample of high signal-to-noise ratio stellar images distributed across the frame.

In the classical theory of third-order aberrations (e.g. Born & Wolf 1980), it is assumed that there is a well-defined optic axis and that deviations from perfect imaging are axially symmetric about this axis. The imperfection can then be described using five numerical coefficients. By measuring the relative displacements of stellar images as a function of the location of the field centre, we can measure one of these coefficients, known as the distortion (e.g. the classic 'barrel' or 'pincushion'). This is a cubic, radial displacement of the images. The two components of the distortion produced two highly significant and independent measurements of the coefficient of distortion: $E = 0.0031 \pm 0.0002$ and $E = 0.0033 \pm 0.0004$. These measurements are consistent with a ray-tracing analysis of the COSMIC optical design using the ZEMAX code, which gives $E = 0.0035$. This distortion corresponds to a radial image displacement of -0.9 arcsec at the centres of the edges of the CCD and -2.6 arcsec at the corners. This distortion is unimportant on the scale of individual faint galaxies. We remove this distortion by geometrically remapping the individual frames before stacking; if we did not do this, the distortion would create artificial polarization in the combined frame of magnitude $\sim(\Delta\theta/10 \text{ arcsec})^2$ per cent, where $\Delta\theta$ is a measure of the frame-to-frame displacement (10–30 arcsec for our data).

The other four aberration coefficients, together with focus errors, deform the image shapes, each with a characteristic pattern. By measuring the variation of the second moments of the stellar images in the M3 frames, we were able to set limits on combinations of these coefficients. (Higher moments are needed to proceed further.) Scaling to a mirror of unit radius (and allowing for occultation by the prime focus cage) and a square CCD of unit half-width, we obtained

$$0.76BC + 0.25F^2 = (1.2 \pm 1) \times 10^{-7},$$
$$0.11C(C + D) = (-1.2 \pm 1) \times 10^{-7}, \quad (6)$$

in the notation of Born & Wolf (1980). There is, therefore, no significant measurement of any additional aberration and we can place an upper limit of 0.01 on any contribution to the mean polarization of galaxy images induced by telescope aberrations. This result is also corroborated by direct ray tracing.

4.2 Atmospheric effects

Atmospheric effects can also produce a spurious ellipticity. The average seeing measured from stars in the combined frames is 0.87 arcsec. Observations were made only near the zenith in order to minimize extinction and also to take advantage of the available seeing. In addition, this aids in reducing the effects of atmospheric refraction. Using the width of the r filter, we calculate that atmospheric refraction should contribute a uniform polarization of no more than 0.006 in a single frame and that the net ellipticity in the combined frame ought to be negligible.

4.3 Guiding errors and atmospheric seeing

Atmospheric seeing effects and telescope guiding errors alter the true shape of a star or galaxy, resulting in the observed image. This can be treated as the convolution of the true image with a point spread function (PSF), which will be non-circular in the case of guiding errors. The artificially induced image ellipticity will be less important for larger images and can, in principle, be removed by extrapolation to infinite image size. If we ignore the influence of sky noise (and, in practice, noise will diminish the apparent size of the faintest galaxies), the observed image second moments, I_{ij}, will be the sums of the second moments associated with the cosmologically distorted images and the PSF.

The complex orientation of an image (galaxy or star) is given by

$$\chi = \frac{\mu_{22} - \mu_{11} - 2\mathrm{i}\mu_{12}}{\mu_{11} + \mu_{22}}, \quad (7)$$

where

$$\mu_{11} = \frac{\int \mathrm{d}x_1\,\mathrm{d}x_2 I^W x_1^2}{\int \mathrm{d}x_1\,\mathrm{d}x_2 I^W} - \left[\frac{\int \mathrm{d}x_1\,\mathrm{d}x_2 I^W x_1}{\int \mathrm{d}x_1\,\mathrm{d}x_2 I^W}\right]^2 \text{ etc.} \quad (8)$$

(Blandford et al. 1991), where $I(x_1, x_2)$ is the surface brightness and the exponent W measures the weight that is given to it. The integrals are carried out over an area defined within a fixed limiting surface brightness. For the CCD data, the integrals are simply replaced by sums over pixels. Note that, to linear order, the modulus of the orientation of a galaxy is equal to its ellipticity as conventionally defined. From Monte Carlo simulations (see Section 4.4) we find little sensitivity to the choice of exponent W above, and so adopt $W = 1$.

The observed complex orientation $\langle\chi\rangle$ expected for images whose sizes are measured by $I_g = I_{11} + I_{22}$ can be

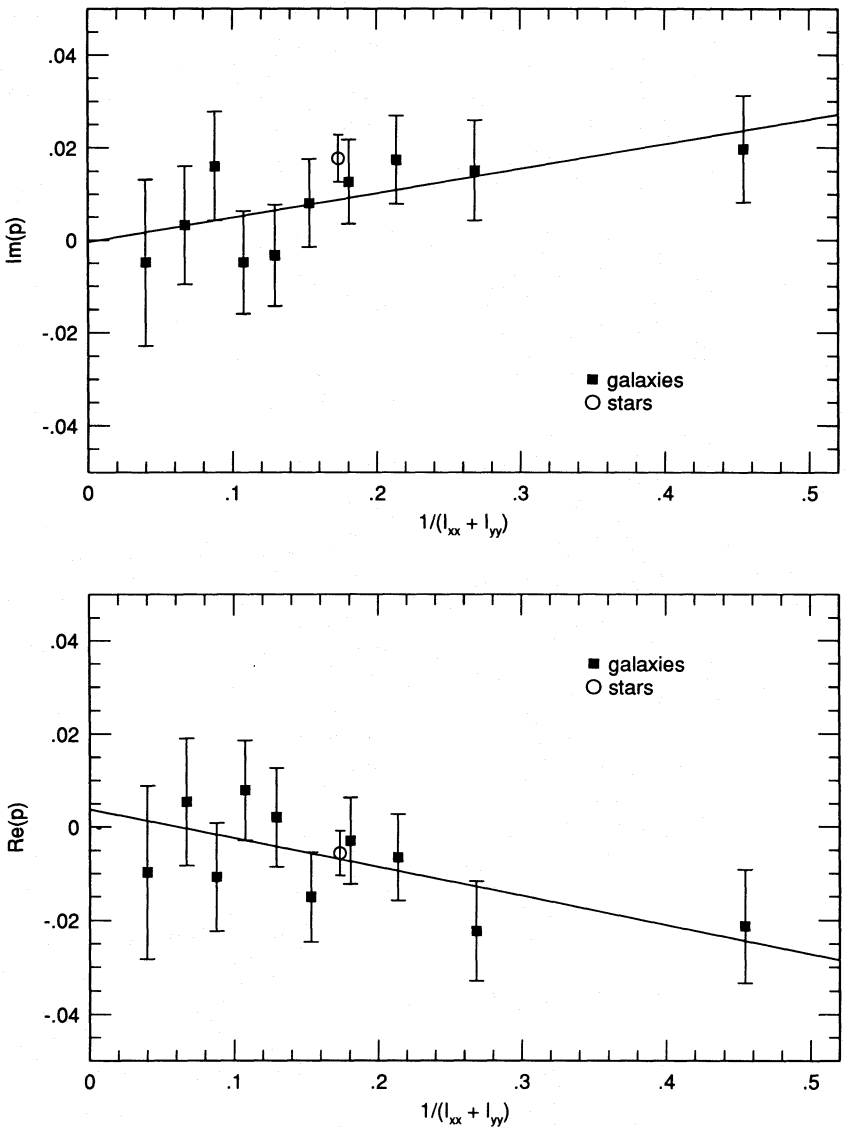

Figure 1. Variation of the real and imaginary parts of the complex orientation of the galaxy (squares) and stellar (circles) images with image size. The error bars correspond to one standard deviation. The linear trend is suggestive of a telescope guiding error in the data. The solid lines show a weighted linear least-squares fit to the galaxy data.

shown to be related to the local (cosmological) polarization p by

$$\langle\chi\rangle(I_g)=p+(\chi_{psf}-p)\frac{I_{psf}}{I_g} \tag{9}$$

to linear order. Here, χ_{psf} is the complex orientation of the point spread function, which can be estimated directly from the stellar images. This formula allows the polarization, p, to be estimated directly from a data set using both the slope and the intercept of a fit of $\langle\chi\rangle$ to $1/I_g$.

We have applied this method to the present data. For the 72 identified stellar images brighter than $r\simeq 24$ found within the central 4.8-arcmin circle, the measured complex ellipticity is found to be

$$\langle\chi\rangle_s=(-0.006\pm0.005)+(0.018\pm0.005)\mathrm{i} \tag{10}$$

(see Fig. 1) and the harmonic mean image stellar second moment is

$$I_s^{-1}=2.2\ \mathrm{arcsec}^{-2}. \tag{11}$$

The 4363 galaxy images with $23<r<26$ and centroids lying within a circular aperture of angular radius 4.8 arcmin centred on the frame were divided into 10 bins on the basis of their second moment sizes, I_g, and the (unweighted) mean complex orientation of the observed galaxy images computed. The bins in I_g were chosen to have equal numbers of galaxy images per bin, resulting in similar standard deviations in the $\langle\chi\rangle$ per bin. Results are shown in Fig. 1. The best fit to relation (9) (also exhibited in Fig. 1) is

$$\langle\chi\rangle(I_g)=[(-0.011\pm0.006)+(0.009\pm0.006)\mathrm{i}]\left(\frac{I_s}{I_g}\right)$$
$$+[(0.004\pm0.007)+(0.0\pm0.007)\mathrm{i}]. \tag{12}$$

By identifying the shape of the stellar image with the PSF, we obtain mean polarization estimates of $\bar{p}=(0.004\pm0.007)+(0.000\pm0.007)$i from the intercept and $\bar{p}=(0.005\pm0.007)+(0.009\pm0.007)$i from the slope of the fit. Combining these two independent estimates, we obtain a formal measurement of

$$\bar{p}=(0.005\pm0.005)+(0.005\pm0.005)\text{i} \quad (13)$$

for the mean polarization of the galaxy images.

This value is predicated upon the particular model of the seeing/guiding correction embodied in equation (9) and the correct identification of the apparently stellar images to define the PSF. A different prescription will give a non-linear extrapolation to infinite image size, and a visual inspection of Fig. 1 suggests that a doubling of the error is appropriate to allow for this possibility, resulting in an upper limit on p of ~ 0.02. This measurement is also dependent upon equal weighting of the galaxy images. A more detailed prescription, in which low-ellipticity images are favoured and which furnishes a significantly different value for the mean image polarization, will be described and critically analysed by Villumsen (in preparation).

An alternative approach to analysing the data is to estimate the two-point polarization correlation function (cf. equation 5) using

$$C_{pp}(\theta)=\langle\chi_i\chi_j^*\rangle \quad (14)$$

averaged over all pairs of galaxies i, j separated by angle θ. Again, all images are weighted equally and the data is divided into five equal θ bins. The results are exhibited in Fig. 2. No significant trend is observed with increasing θ. The formal, θ-averaged measurement is

$$C_{pp}=(1.4\pm3.0)\times10^{-5}. \quad (15)$$

The data were also divided into two isophotal area bins (0.63 to 3.2 arcsec^2, median magnitude of $r=25.6$; 3.2 to 27.1 arcsec^2, median magnitude of $r=24.6$). No significant trend of C_{pp} with isophotal image size is seen (cf. Fig. 2).

The flatness of C_{pp} puts limits on the strength of the five classical aberrations in the data. An aberration signal that increases away from the optic axis will lead to a steeply decreasing $C_{pp}(\theta)$. On scales much smaller than the size of the frame, galaxies will tend to point in the same direction, leading to a large positive value of C_{pp}. On scales larger than about half the frame, galaxies will tend to be perpendicular to each other, leading to a negative value of C_{pp}. The observed flatness of C_{pp} indicates that classical aberrations are not a serious problem in this data (confirming the conclusions of Section 4.1).

4.4 Monte Carlo simulations

While low-order telescope aberrations and atmospheric effects can be calibrated and removed from the data set, other effects cannot be easily compensated for, and it is necessary to perform Monte Carlo simulations to quantify their contributions to the overall error budget.

Simulated frames were created from catalogues of images with random orientations and positions. The surface-brightness profiles were taken to be exponential discs, which

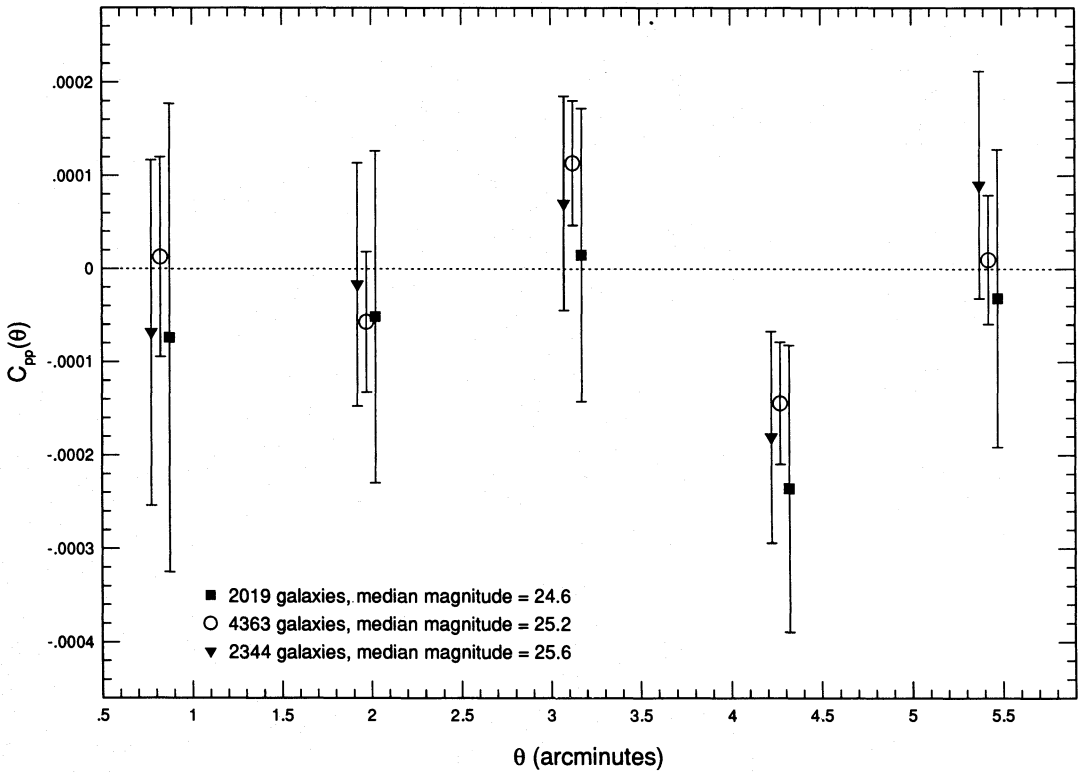

Figure 2. C_{pp} as a function of angular separation for our complete sample with $23\leq r\leq26$ (circles) and also for this sample split on the basis of isophotal image area (small images: triangles; large images: squares). Median magnitudes are quoted for all samples.

appear to dominate in high-resolution imaging of the faint field population at brighter magnitudes (e.g. Ellis 1993). The galaxy parameters (magnitudes, scale sizes and ellipticities) were chosen such that the distributions of these parameters, after the simulated images were convolved with the seeing, matched the observed distributions. The surface density of objects above our completeness limit was matched to that observed (64 per arcmin^2) and, in addition, fainter galaxies were added by extrapolating the number counts two magnitudes fainter in order to simulate the effects of crowding and merging of these undetected faint galaxies on the detected objects. A small fraction (~ 1 per cent) of stellar sources were added to calibrate the seeing.

The initially random galaxy images were sheared coherently with a constant, known polarization, after which the images were pixellated and convolved with the point spread function defined by the telescope and atmosphere. Finally, sky noise was added to obtain the same detection limit as in the real images. The sky noise was correlated across pixels to simulate the resampling that occurs during the image reduction. These simulated frames were then analysed using the procedure described above for the actual data set.

Four independent realizations were generated for each of four known 'input' polarizations, and simulated galaxy catalogues were obtained. The input polarizations ranged from cosmologically 'reasonable' ($p \simeq 0.035$) to 'unreasonable' ($p \simeq 0.11$). The mean polarization, $\overline{p}$, of the simulated $23 \leq r \leq 26$ galaxies in each independent catalogue was measured in the same manner in which $\overline{p}$ was measured for the actual data set. These simulations show a linear trend between the output $\overline{p}$ and the value input into the simulation. However, the measured output value of the mean polarization is of the order of 40 ± 10 per cent of the input polarization, illustrating the relative inefficiency of the signal detection with our current data set. Roughly one-third of the signal attenuation is associated with image crowding, pixellation and inefficiencies in the FOCAS object detection and shape analysis; the remainder is attributable to seeing and sky noise.

As an illustration of the importance of adequate seeing, one simulation of a deep r exposure taken in 0.5-arcsec seeing was performed. The observational parameters of this simulation were those of a 2-h exposure using the low-resolution imaging spectrograph (LRIS) on the 10-m Keck Telescope, although it could equally well represent a longer exposure on any 4-m class telescope at a good site (e.g. the Canada–France–Hawaii Telescope). This simulation reaches a similar depth to that of our data set over a 6×8 arcmin^2 field, and we find we can efficiently recover a uniform cosmological polarization of $p = 0.035$ in the presence of *both* seeing and sky noise. The signal detection efficiency is ~ 80 per cent, roughly double that of the current observational data set. The efficiency of the signal detection in 0.5-arcsec seeing is close to optimal for the depth of the simulated observation, given the effects of image crowding and the object detection algorithm.

The simulations also aid in determining the most efficient weighting for the image moment (i.e. the exponent W introduced in Section 4.3). Little sensitivity to the choice of W was found, and a choice of $W = 1$ was adopted. In addition, we varied the source surface-brightness profiles and found that irregular images (i.e. intrinsically 'clumpy' surface-brightness profiles as opposed to smooth exponentials) yielded similar results.

5 DISCUSSION AND CONCLUSIONS

We determine a value of $\overline{p} = 0.01 \pm 0.01$ for the mean polarization of the faint galaxies ($23 \leq r \leq 26$) in our data set within a 4.8-arcmin radius aperture after correcting for the distortion aberration and guiding error as described above. The associated two-point polarization correlation function, $C_{pp}(\theta)$, of these galaxies was found to be $(1.4 \pm 3.0) \times 10^{-5}$, independent of θ and isophotal image size.

The Monte Carlo simulations suggest that, for the atmospheric seeing and sky noise associated with our data set, the efficiency of measuring a cosmologically induced correlated ellipticity of the faint galaxies is of order 40 ± 10 per cent. This result suggests that our data yield an upper limit on the strength of weak gravitational lensing by large-scale structure in the Universe of $\overline{p}_{max} \simeq 0.04$.

As a specific example of a model for the dominant mass component of the Universe, we have chosen the standard CDM model, which predicts that the cosmological polarization of faint galaxy images should be in the range $\overline{p} = 0.03 \pm 0.01$. Thus, while not particularly strong, our upper limit on $\overline{p}$ falls in a cosmologically interesting range.

If it is possible to obtain unaberrated imaging in ~ 0.5-arcsec seeing with an instrument such as LRIS on the 10-m Keck telescope, our Monte Carlo simulations suggest that a relatively short exposure of a single blank field would yield a strong limit on the amount of weak gravitational lensing of distant galaxies by large-scale structure.

ACKNOWLEDGMENTS

We thank Alan Dressler for leading the construction of the COSMIC camera and Simon Lilly, Nick Kaiser and Tony Tyson for advice and encouragement. Support under NSF grants AST-89-17765 (RDB, TGB), AST 92-23370 (RDB, TGB), AST-89-13664 (TGB), AST-89-21001 (JVV), the Ohio Supercomputer Center (JVV), a NATO Postdoctoral Fellowship (IRS), and an NSF Graduate Fellowship (TAS) is gratefully acknowledged.

REFERENCES

Binggeli B., 1982, A&A, 107, 338
Blandford R. D., Jaroszyński M., 1981, ApJ, 246, 1
Blandford R. D., Narayan R., 1992, ARA&A, 30, 311
Blandford R. D., Saust A. B., Brainerd T. G., Villumsen J. V., 1991, MNRAS, 251, 600
Born M., Wolf E., 1980, Principles of Optics. Pergamon Press, Oxford
Brainerd T. G., Villumsen J. V., 1994, ApJ, 425, 403
Davis M., Efstathiou G., Frenk C. S., White S. D. M., 1985, ApJ, 292, 371
Dressler A., Kells W., 1993, COSMIC manual. Observatories of the Carnegie Institution of Washington, Pasadena
Ellis R. S., 1993, in Soifer B. T., ed., ASP Conf. Ser. Vol. 43, Sky Surveys: Protostars to Protogalaxies. Astron. Soc. Pac., San Francisco, p. 165
Fort B., Le Borgne J. F., Mathez G., Mellier Y., Picat J. P., 1991, Ann. Physique, 16, 211
Guhathakurta P., Tyson J. A., Majewski S. R., 1990, ApJ, 357, L9
Gunn J. E., 1967, ApJ, 150, 737

Huchra J., Geller M., De Lapparent V., Burg R., 1988, in Audouze J., Pelleton M.-C., Szalay A., eds, Proc. IAU Symp. 130, Large-Scale Structures of the Universe. Kluwer, Dordrecht, p. 105
Jarvis J. F., Tyson J. A., 1981, AJ, 86, 476
Kaiser N., 1992, ApJ, 388, 272
Kristian J., 1967, ApJ, 147, 864
Lilly S. J., 1993, ApJ, 411, 501
Lilly S. J., Cowie L. L., Gardner J. P., 1991, ApJ, 369, 79
Metcalfe N., Shanks T., Roche N., Fong R., 1993, in Akerlof C. W., Srednicki M. A., eds, Relativistic Astrophysics & Particle Cosmology. Ann. New York Acad. Sci. Vol. 688, p. 534
Miralda-Escudé J., 1991, ApJ, 380, 1
Saunders W., Frenk C., Rowan-Robinson M., Efstathiou G., Lawrence A., 1991, Nat, 349, 32
Schneider P., Ehlers J., Falco E. E., 1992, Gravitational Lensing. Springer-Verlag, Berlin
Smail I., Ellis R. S., Fitchett M. J., 1994, MNRAS, 270, 245
Smoot G. F., Bennett C. L., Kogut A., Wright E. L., 1992, ApJ, 396, L7
Steidel C. C., Hamilton D., 1993, AJ, 105, 2017
Tyson J. A., 1988, AJ, 96, 1
Tyson J. A., Valdes F., Wenk R. A., 1990, ApJ, 349, L1
Valdes F., Tyson A. J., Jarvis J. F., 1983, ApJ, 271, 431
Walsh D., Carswell R. F., Weymann R., 1979, Nat, 279, 381
Zwicky F., 1937, Phys. Rev. Lett., 51, 679